Development 139, 2371-2380 (2012) doi:10.1242/dev.079806

Hedgehog-dependent proliferation drives modular growth during morphogenesis of a dermal bone

Tyler R. Huycke, B. Frank Eames* and Charles B. Kimmel‡

SUMMARY

In the developing skeleton, dermal bone morphogenesis includes the balanced proliferation, recruitment and differentiation of osteoblast precursors, yet how bones acquire unique morphologies is unknown. We show that Hedgehog (Hh) signaling mediates bone shaping during early morphogenesis of the opercle (Op), a well characterized dermal bone of the zebrafish craniofacial skeleton. *ihha* is specifically expressed in a local population of active osteoblasts along the principal growing edge of the bone. Mutational studies show that Hh signaling by this osteoblast population is both necessary and sufficient for full recruitment of pre-osteoblasts into the signaling population. Loss of *ihha* function results in locally reduced proliferation of pre-osteoblasts and consequent reductions in recruitment into the osteoblast pool, reduced bone edge length and reduced outgrowth. Conversely, hyperactive Hh signaling in *ptch1* mutants causes opposite defects in proliferation and growth. Time-lapse microscopy of early Op morphogenesis using transgenically labeled osteoblasts demonstrates that *ihha*-dependent bone development is not only region specific, but also begins exactly at the onset of a second phase of morphogenesis, when the early bone begins to reshape into a more complex form. These features strongly support a hypothesis that dermal bone development is modular, with different gene sets functioning at specific times and locations to pattern growth. The Hh-dependent module is not limited to this second phase of bone growth: during later larval development, the Op is fused along the dysmorphic edge to adjacent dermal bones. Hence, patterning within a module may include adjacent regions of functionally related bones and might require that signaling pathways function over an extended period of development.

KEY WORDS: Dermal bone, Hedgehog signaling, Modularity, Morphogenesis, Skeletogenesis, Zebrafish

INTRODUCTION

During formation of the skeleton, bones and cartilages with unique morphologies are produced to provide structural support and framework for the body and protection to vital organs. Understanding the regulation of bone morphogenesis, the acquisition of form through shape and/or size changes, is of particular interest as alterations to these controls can result in skeletal defects in human inherited disorders and might drive morphological change during vertebrate evolution (Zelzer and Olsen, 2003; Kimmel et al., 2007).

The shape of dermal bones (i.e. those that develop from the direct differentiation of mesenchymal cells into osteoblasts) is especially dependent upon two important developmental events: condensation and osteoblast recruitment. This dependence is highlighted by the fact that the shape and size of mesenchymal condensations, groups of previously unorganized cells prior to overt differentiation into bone-forming osteoblasts, is predictive of early bone morphology (Hanken and Hall, 1993; Hall and Miyake, 2000; Eames et al., 2003). After the condensation has formed, bone shaping is thought to be controlled through the recruitment of new osteoblasts to the growing bone in a space- and time-dependent manner (Kimmel et al., 2010). Nevertheless, the molecular determinants that regulate dermal bone shape throughout development remain obscure, in part because dermal bone morphogenesis is complex and involves multiple developmental origins and processes over long periods of time.

To understand such complex bone morphogenesis, researchers have long used the rodent mandible as a model (Atchley and Hall, 1991; Hanken and Hall, 1993). The dermal bone component of the mandible grows appositionally: differentiating osteoblasts surrounded by their proliferating progenitors line the pre-existing bone surfaces (Atchley and Hall, 1991; Ramaesh and Bard, 2003). Mandibular morphogenesis occurs over a long period of development, and interactions of the osteogenic tissues with teeth and muscle are important for its later form and functional integrations (Atchley and Hall, 1991). Furthermore, it is hypothesized that the mandibular dermal bone comprises two distinct morphogenetic components, the anterior alveolar region and the posterior ascending ramus (Atchley and Hall, 1991; Hanken and Hall, 1993; Klingenberg et al., 2003; Klingenberg, 2009). These independent components, or modules, are characterized as having strong internal integration, but only sharing weak interactions with other modules (Raff, 1996; von Dassow and Munro, 1999; Wagner et al., 2007; Klingenberg, 2009). Developmental modularity might allow different signaling pathways to regulate the rates of growth independently within each module at specific times, allowing for precise regulation of bone shape. However, even though many genes are involved in mandibular formation (Bronner et al., 2010), no functional evidence exists that demonstrates how specific molecular activities can impose such regulation.

Here, we use the zebrafish opercle (Op) as a model system for understanding at cellular resolution the genetic regulation of growth and shaping of bone. The Op, a neural crest-derived dermal bone in the second pharyngeal arch, undergoes a series of

Institute of Neuroscience, University of Oregon, Eugene, OR 97403, USA.

*Present address: Department of Anatomy and Cell Biology, University of Saskatchewan, Saskatoon, SK S7N 5E5, Canada
‡Author for correspondence (kimmel@uoneuro.uoregon.edu)

Accepted 23 April 2012

characterized shape changes during larval development (Kimmel et al., 2010). Initial ossification of the Op occurs through the formation of a linear spur of bone matrix surrounded by osteoblasts that projects ventrally away from the joint it forms with the hyosymplectic cartilage (Cubbage and Mabee, 1996; Kimmel et al., 2010). Further morphogenesis of the Op throughout larval development occurs allometrically, with shape and size changes accompanied by new osteoblast arrangements and localized deposition of mineralized matrix along the pre-existing surfaces of the bone (Kimmel et al., 2010). Mutational analyses have identified genes in the endothelin 1 signaling pathway, particularly *edn1* and its effectors, Dlx genes and *mef2ca*, to be crucial determinants of Op shape (Kimmel et al., 2003; Walker et al., 2006; Miller et al., 2007). The specific timing of Op growth and shape changes implies that Op morphogenesis is modular (Kimmel et al., 2010), and we take a genetic approach to test this hypothesis and address how molecular determinants fine tune bone shape.

We identify *indian hedgehog a* (*ihha*), encoding a Hedgehog (Hh) family ligand, and *patched 1* (*ptch1*; formerly *ptc2* – Zebrafish Information Network), encoding a Hh receptor, as key regulators of Op morphogenesis. Our data provide genetic evidence that the bone-shaping process is regulated in a modular fashion, as *ihha* and *ptch1* mutants display spatially localized defects in Op growth. Through time-lapse analysis of Op development at cellular resolution, we show that Hh signaling is required regionally for the proper rate of nascent osteoblast addition to the growing bone. Furthermore, we find that levels of Hh signaling activity positively correlate with amounts of cell proliferation along the ventral Op edge. Finally, fusions of the Op and adjacent dermal bones in *ihha* mutants indicate that the Hh-dependent module may extend locally to immediately adjacent regions of separate bones.

MATERIALS AND METHODS

Zebrafish lines

Zebrafish were reared according to standard protocols (Westerfield, 2007) and staged as previously described (Kimmel et al., 1995; Parichy et al., 2009). All experiments conducted were approved by the University of Oregon Institutional Animal Care and Use Committee (IACUC). Zebrafish lines were as described: *ihha*^{hu2131} (Parkin et al., 2009), *ptch1*^{tj222} (Koudijs et al., 2005), *Tg(sp7:EGFP)b1212* (DeLaurier et al., 2010) and *trps1*^{J1271aGt} (Talbot et al., 2010). *ihha* mutants were identified by PCR genotyping with the primers ihhaf6 (5′-CTGTGCCACCGTACCACTC-3′) and ihhar5 (5′-GCTACATTTGGACTAAACTGCAT-3′), and wild-type allele cut with *Nsp*I. *ptch1* mutants were genotyped with the primers lepf6 (5′-TGGAAACCTGGCTACTTTTTG-3′) and lepr5 (5′-AAAGCGGCGGTCCTCTCTTCG-3′), and wild-type allele cut with *Taq*αI.

Live Alizarin Red and calcein staining

Skeletal staining was performed as previously described (Kimmel et al., 2010). For single-labeling experiments, larvae of all ages were stained overnight in the dark with 50 μg/ml Alizarin Red in E2 embryo medium. For double labeling experiments, larvae were incubated in 50 μg/ml Alizarin Red and 10 mM HEPES in E2 for 2 hours at 5 dpf and 50 μg/ml calcein at 7 dpf before being imaged at 8 dpf.

Cyclopamine treatment

Larvae were treated with cyclopamine (Toronto Research Chemicals) as previously described (Winata et al., 2009). Larvae were exposed to 100 μM cyclopamine/1% ethanol in E2 from 4-6 dpf. Controls were treated with 1% ethanol in E2.

EdU chemistry, TUNEL assay and nuclear staining

Larvae (4 dpf) were incubated from 4-5 dpf in 1 mM EdU (5-ethynyl-2′-deoxyuridine) in E2. Larvae were then anesthetized and fixed overnight at 4°C in 4% PFA/1×PBS. Following fixation, fish were washed with PBSTx (1% Triton X-100/1× PBS) and incubated with anti-GFP Alexa Fluor 488 (Invitrogen) 1:500 in PBSTx overnight at 4°C. After several washes in PBSTx, the Click-iT (Invitrogen) EdU reaction mixture was made according to manufacturer's instructions and larvae were incubated in the reaction mixture for 1 hour. Apoptotic cells were labeled by TUNEL using the in situ cell death detection kit with TMR red (Roche) as previously described (Wu et al., 2006). For cell labeling, larvae were fixed overnight in 4% PFA/1×PBS, permeabilized with PBSTx and incubated with SYTO-59 (Invitrogen) at a 1:1000 dilution in PBSTx for 1 hour.

RNA fluorescent in situ hybridization

Zebrafish were reared in 15 mg/l PTU (1-phenyl-2-thiourea). Whole-mount labeling was performed essentially as described (Talbot et al., 2010). Larvae (5 dpf) were permeabilized with 10 μg/ml Proteinase K in PBST at room temperature for 45 minutes. Probes used have been described previously: *ihha* and *col10a1* (Avaron et al., 2006), *ihhb* (Currie and Ingham, 1996), *ptch1* (Lewis et al., 1999), *ptch2* (Concordet et al., 1996), *sp7* (DeLaurier et al., 2010), *gli1* (Karlstrom et al., 2003), *gli2a* (Karlstrom et al., 1999), *gli3* (Tyurina et al., 2005), and *runx2a* and *runx2b* (Flores et al., 2004).

Microscopy and measurements

Imaging was conducted using either a Zeiss LSM 5 Pascal confocal or Leica SD6000 spinning disk confocal with Borealis illumination technology. For time-course analysis, fish from a single clutch were only used for imaging at one stage to prevent stress-induced developmental delay. Opercle length measurements were obtained using ImageJ (National Institute of Health). For time-lapse imaging, larvae were anesthetized in 80 mg/l clove oil (Hilltech), mounted in 0.4% agarose in glass-bottomed Petri dishes, covered with E2 containing clove oil, and imaged at 30 minute intervals. Larvae imaged in this manner appeared similar to staged, non-imaged controls. Movies were constructed from z-projections using Metamorph imaging software (Molecular Devices). Quantitation of osteoblast addition was conducted manually across individual sections from time-lapse movies. The anterior and posterior halves of the Op are defined by the major axis of a best fit ellipse to each individual bone.

For time-lapse alignments, stacks of *z*-projections were aligned at 3 dpf by the joint and angle of the linear Op using ImageJ. The resultant channels were then thresholded individually at each stage. The area within the thresholded Op was filled using the fill hole command in ImageJ. Four regions of interest were constructed on the aligned Op based on divisions created using the draw ellipse macro in ImageJ. Percent overlap between images for each region of interest was calculated on the threshold, aligned images using the colocalization threshold plug-in.

Morphometric analysis

Morphometric analysis was performed on a series of 14 digitized and Procrustes aligned landmarks on the Op shown in Fig. 1I, essentially as previously described (Kimmel et al., 2010). The 11 landmarks between the three apices along the bone were treated as sliding semi-landmarks. Visualizations of the landmark configurations as wire-frame diagrams, Principal component analysis and discriminant function analysis were implemented in MorphoJ version 1.02f (Klingenberg, 2011). For the presentation in Fig. 1I, the shape configurations were taken out of Procrustes alignment by scaling to their correct (non-normalized) sizes and manually aligning to the joint region, where bone growth initiates (Kimmel et al., 2010).

RESULTS

Opercle morphogenesis is altered in *ihha* mutants

The opercle (Op) of zebrafish larvae homozygous for the putative null *ihha*^{hu2131} allele (Parkin et al., 2009) is malformed in shape and reduced in size compared with wild type (Fig. 1A,B). To investigate the developmental basis of the morphological defects, we performed a systematic analysis of early larval Op development in *ihha* mutants carrying the *sp7:EGFP* transgene, which labels osteoblasts (DeLaurier et al., 2010). The Op forms a linear spur

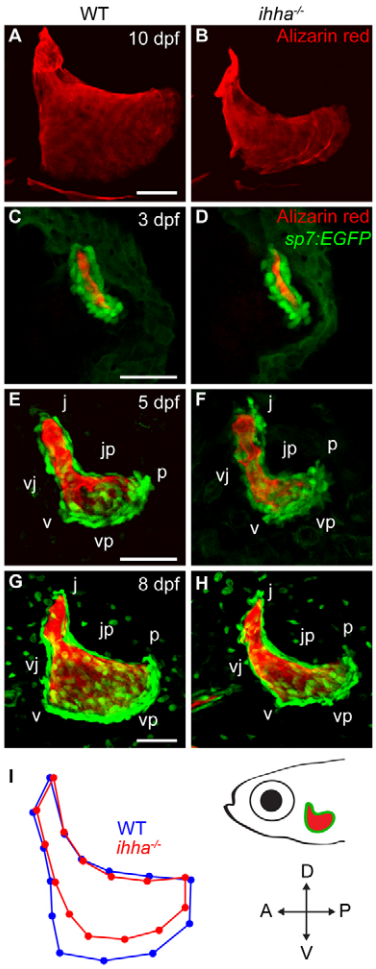

Fig. 1. *ihha* is required for proper Op morphogenesis. Confocal projections and morphometric analysis of the Alizarin Red-stained Op in live wild-type and *ihha* mutant zebrafish larvae expressing *sp7:EGFP* (C-H). Images are lateral views with dorsal upwards and anterior towards the left. (**A**,**B**) The Op is mis-shapen and reduced in dorsoventral length in *ihha* mutants. (**C**,**D**) The *ihha* mutant Op has wild-type morphology at 3 dpf. (**E-H**) The *ihha* mutant Op is malformed at 5 and 8 dpf. (**I**) Average configuration of landmarks from morphometric analysis of the Op for *n*=23 wild type (blue) and *n*=22 *ihha* mutants (red) shows shape differences anterior and ventral to the v apex. The centroid size of the Op calculated from the same set of data is significantly smaller in *ihha* mutants (one-way ANOVA mean±s.e.m.: wild type=0.198±0.00544; *ihha*=0.181±0.00532, *P*=0.0293). j, joint apex; p, posterior apex; v, ventral apex; jp, edge connecting j and p; vj, edge connecting v and j; vp, edge connecting v and p. Scale bars: 50 µm.

surrounded by *sp7:EGFP*-expressing osteoblasts at 3 days post fertilization (dpf) in wild type (Kimmel et al., 2010) and is unchanged in *ihha* mutants (Fig. 1C,D). Expansion of the ventral edge from 3-5 dpf forms a triangular Op, bounded by edges jp, vj and vp (Fig. 1E) (Kimmel et al., 2010). At 5 dpf, Op morphology is altered in *ihha* mutants: there are fewer osteoblasts near the v apex (Fig. 1F). Growth at this stage results in an overall size increase of the Op by 8 dpf (Fig. 1G), but *ihha* mutants display an apparent reduction in both osteoblasts and bone near the v apex (Fig. 1H). The shaping of other craniofacial dermal bones appears unaltered at this time, suggesting that *ihha* uniquely regulates Op morphology (data not shown).

Geometric morphometrics with landmarks placed along the Op edges (Kimmel et al., 2010) allows us to assess bone size and shape deformations quantitatively in *ihha* mutants. Mean centroid size of the *ihha* mutant Op is significantly smaller than that of the wild-type Op (Fig. 1I), and the mean shape difference appears as a local reduction of the ventral region of the bone near the v apex (Fig. 1I), matching our interpretations described above. Principal component analysis shows a clear separation in Op shapes of wild types and *ihha* mutants along the principal axis of shape variation (supplementary material Fig. S1). Furthermore, Procrustes distance, a univariate measure of shape disparity between the two groups, is substantial and highly significant. These results demonstrate that *ihha* is a key regulator of Op size and shape.

ihha regulates localized osteoblast addition and vp edge length

We used confocal time-lapse imaging of larvae with transgenically labeled osteoblasts from 3-4 dpf to examine the function of *ihha* at the cellular level in Op morphogenesis. In both wild-type and *ihha* mutant larvae, early Op morphogenesis occurs mainly through the addition of nascent (i.e. newly expressing) *sp7:EGFP*-expressing cells to the ventral edge of the linear spur, rather than by division of pre-existing *sp7:EGFP*-expressing cells (supplementary material Movies 1-3). Quantitation of the rate of nascent *sp7:EGFP*-expressing osteoblast addition to the Op reveals a spatially localized deficit in cells added to the anteroventral Op edge in *ihha* mutants (Fig. 2A). Direct comparison by alignment of time-lapse movies reaffirms that at first (3 dpf) the *ihha* mutant Op has wild-type morphology (Fig. 2B; supplementary material Movies 1, 2). The wild-type Op enters a second phase of morphogenesis between 3 and 3.5 dpf, indicated by the onset of osteoblast addition to both the anterior and posterior sides of the ventral tip, resulting in a fan-shaped array of osteoblasts (supplementary material Movies 1, 2). By 3.5 dpf and increasingly evident at 4 dpf, *ihha* mutants have fewer cells along the anterior of the ventral edge in comparison with wild type (Fig. 2C,D, arrows; supplementary material Movies 1, 2). This variation is not observed between alignments of two wild-type Ops (supplementary material Movie 3).

To verify our observation that defects in osteoblast addition in *ihha* mutants result in a region-specific Op shape change, we used aligned time-lapse images to calculate the fraction of wild-type EGFP-derived fluorescence overlapping with that of *ihha* mutant larvae in quadrants defined by the major and minor axes of a best fit ellipse to the Op (WT:ihha). As a control for variation in wild-type development, we also compared overlapping fluorescence between pairs of aligned wild-type larvae (WT:WT). The WT:ihha percent overlap at 3 dpf is not significantly different from WT:WT in any quadrant (Fig. 2E). *ihha* mutant Op shape is distinct from wild type at 3.5 and 4 dpf, specifically in the anteroventral quadrant, matching our observations above (Fig. 2F,G). At no time points are any other quadrants affected (Fig. 2E-G). Thus, the effects of *ihha* loss are specific in space and time.

The major modes of growth during larval Op morphogenesis are extensions in length along the vj, jp and vp edges at precise times (Fig. 1) (Kimmel et al., 2010). We thus tested whether the early defects in cell addition along the vp edge in *ihha* mutants cause a specific shortening of this edge. Quantitation of Op edge lengths supports this idea, revealing a significant reduction in vp edge length in *ihha* mutants, but no change in vj or jp (Fig. 3A-E). Furthermore, double labeling of the Op bone matrix at 5 dpf with Alizarin Red and then at 8 dpf with another calcified bone label,

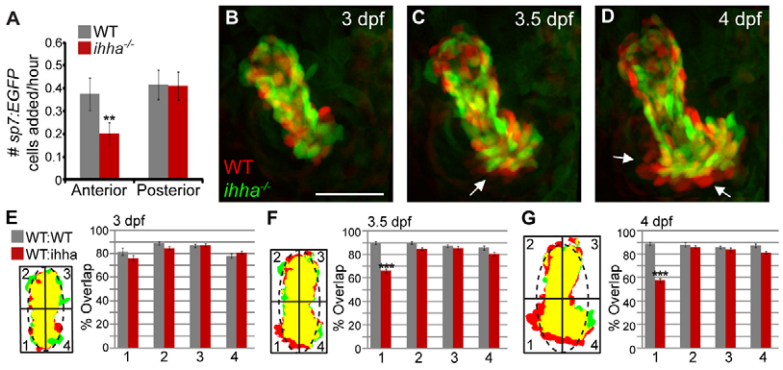

Fig. 2. *ihha* is required for regional Op growth through cell addition. Aligned and overlapping confocal projections of a wild-type Op (red) and an ihha mutant Op (green) from a time-lapse of *sp7:EGFP*-expressing larvae (see supplementary material Movie 1) reveal early shape changes due to reduced cell addition. Images are lateral views with dorsal upwards and anterior towards the left. (**A**) Quantitation of peripheral osteoblast addition to the anterior and posterior halves of the Op from 3-4 dpf shows decreased anterior, but not posterior, cell addition. (**B-D**) Osteoblasts are added to the anteroventral region of the wild-type Op after 3 dpf (arrows) but are lacking in *ihha* mutants. (**E-G**) Threshold images derived from A-C showing separation of the Op into quadrants by a best-fit ellipse (broken line). Alignments are accompanied by graphs representing the fraction of wild-type Op that overlaps with *ihha* mutant Op (WT:ihha, 36 comparisons) or the fraction of wild-type Op overlapping with another wild-type Op (WT:WT, 21 comparisons) for each quadrant/time point. (E) WT:ihha overlap at 3 dpf is not significantly different from WT:WT overlap. The anteroventral edge (quadrant 1) shows a significant reduction in WT:ihha overlapping area at 3.5 dpf (F) and 4 dpf (G), but other quadrants are not significantly altered. Data are presented as mean±s.d., $**P<0.01$ by unpaired *t*-test, $n\geq7$ per genotype (A); and mean±s.e.m. $***P<0.001$ by Tukey-Kramer method following one-way ANOVA, $n=6$ per genotype in E-G. Scale bar: 50 μm.

calcein, demonstrates that the reduction in ventral outgrowth is localized to the vp edge (Fig. 3F,G). Posterior outgrowth of the vp edge near the posterior (p) apex is relatively unaltered (Fig. 3F,G). Overall, these data support a model in which *ihha* coordinates morphogenesis within a specific ventral region of the Op by promoting local cell addition and bone extension exclusively along the vp edge.

ihha is required for normal levels of proliferation along the vp edge

As Hh signaling has been shown to promote proliferation of chondrocytes as well as of a variety of other cell types (St-Jacques et al., 1999; Long et al., 2001; Agathocleous et al., 2007; Hammond and Schulte-Merker, 2009), we asked whether Hh signaling controls cell addition and vp edge length by regulating the rate of cell proliferation. In wild-type larvae at 5 dpf, many proliferative cells just ventral to and including the *sp7:EGFP*-expressing vp edge osteoblasts are EdU positive following a 24 hour incubation (Fig. 4A). *ihha* mutants show a significant decrease in EdU-labeled cells in both *sp7:EGFP*-expressing vp edge osteoblasts and in *sp7:EGFP*-negative cells within two cell diameters of the vp edge (Fig. 4B,C). The total number of cells in this region is decreased by ~30% in *ihha* mutants at 5 dpf; however, the number of proliferating cells is reduced by 60-70%, and therefore the decrease in cells cannot completely account for reduced proliferation (Fig. 4C; data not shown). Interestingly, the reduction in total cells correlates exactly with the 30% reduction in vp edge length apparent at this time (Fig. 3, Fig. 4C). Notably, *ihha*

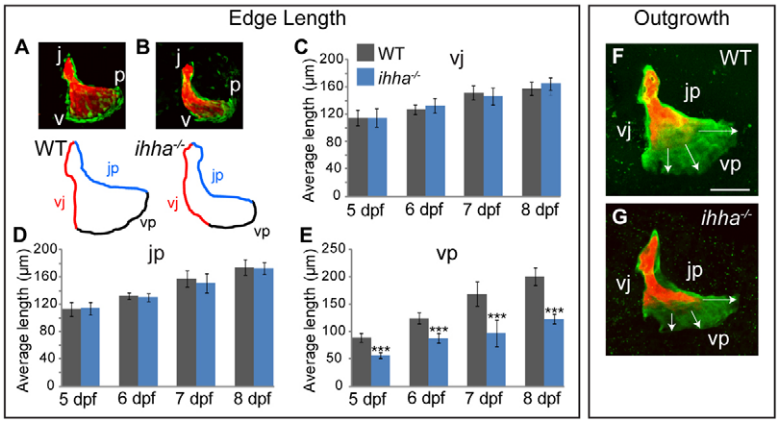

Fig. 3. Growth along the vp edge is regulated by *ihha*. Quantitation of Op edge lengths and outgrowth. Images are lateral views with dorsal upwards and anterior towards the left. (**A**,**B**) Images and drawn outlines of the 7 dpf Op showing the vj, jp, and vp edges as defined by Alizarin Red and *sp7:EGFP*-expressing osteoblast localization (see Fig. 1). (**C-E**) vp edge length is significantly reduced in *ihha* mutants (E), whereas jp (D) and vj (C) edge lengths are unchanged. (**F**,**G**) Double labeling of the Op at 5 dpf with Alizarin Red and at 8 dpf with calcein (green) indicates specifically reduced ventral Op outgrowth in *ihha* mutants. Data are presented as mean±s.d., $***P<0.001$ by unpaired *t*-test, $n\geq7$ per genotype/timepoint. Images in F and G are representative of $n\geq6$ larvae per genotype. v, ventral apex; p, posterior apex; j, joint apex; vp, edge connecting v and p; vj, edge connecting v and j; jp, edge connecting j and p. Scale bar: 50 μm.

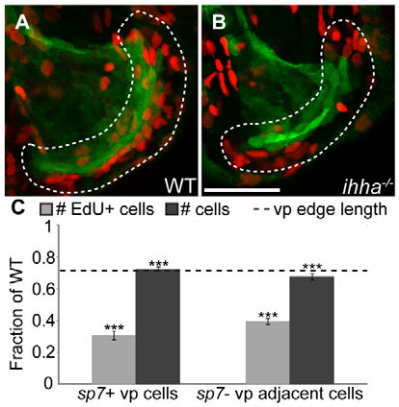

Fig. 4. *ihha* controls cell proliferation. Quantitation of cell proliferation in *ihha* mutants and wild-type siblings. Images are lateral views with dorsal upwards and anterior towards the left. (**A**,**B**) Confocal projections of the Op at 5 dpf showing *sp7:EGFP*-expressing osteoblasts (green) and EdU-positive (EdU+) cells (red). (A) EdU+ cells are mostly found along the actively growing vp edge in wild type. (B) Fewer EdU+ cells are apparent along the vp edge in *ihha* mutants. Scale bar: 50 μm. (**C**) Quantitation of EdU+ cells along the vp edge as a fraction of wild-type levels shows that the amount of EdU+ cells is significantly decreased in *ihha* mutants. Cells included in the count, represented by dashes in A and B, are those within two cell diameters of the vp edge that express *sp7:EGFP* (*sp7*+ vp cells) or those that do not (*sp7*–, vp adjacent cells). The number of total cells stained with SYTO-59 was counted with the same parameters in a separate experiment and is decreased to a lesser extent than the number of EdU+ cells, but proportional to the decrease in vp edge length (shown as a broken line and based on Fig. 3). Data are presented as mean±s.e.m., ***P<0.001 by unpaired t-test, n≥10 per genotype.

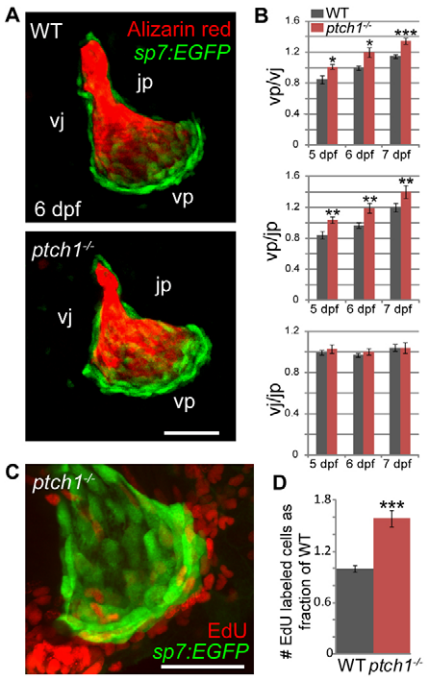

Fig. 5. *ptch1* represses bone growth and proliferation. Quantitation of Op edge lengths and cell proliferation in *ptch1* mutants. Images are lateral views with dorsal upwards and anterior towards the left. (**A**) Confocal projections of *ptch1* mutants and wild-type siblings carrying the *sp7:EGFP* transgene at 6 dpf demonstrate an apparent elongation of the vp edge in *ptch1* mutants. (**B**) vp/jp and vp/vj ratios are significantly greater in *ptch1* mutants relative to wild-type siblings. Conversely, the vj/jp ratio is unaffected in *ptch1* mutants. (**C**,**D**) *ptch1* mutants display a significant increase in EdU-positive cells within two cell diameters of the vp edge at 5 dpf (compare with wild type in Fig. 4 as number of proliferating cells in wild-type larvae was similar between the two experiments). Note that neuromast cells that are occasionally apparent near the v apex were not included in the count. Data are presented as mean±s.e.m., *P<0.05, **P<0.01, ***P<0.001 by unpaired t-test, n≥7 per genotype/age. v, ventral apex; p, posterior apex; j, joint apex; vp, edge connecting v and p; vj, edge connecting v and j; jp, edge connecting j and p. Scale bars: 50 μm.

mutants show no significant change in the number of EdU-positive cells dorsal to the Op in a region that is likely to be occupied by Op-associated muscles (data not shown), indicating that *ihha* mutants do not have decreased proliferation throughout the entire animal. We saw no significant change in cell death by a TUNEL assay (data not shown). These data provide evidence that reduced osteoblast addition to the *ihha* mutant Op is due to locally decreased cell proliferation.

ptch1 positively regulates vp edge length and proliferation

The Hh receptor *ptch1* (formerly *ptc2*) is a negative regulator of Hh signaling, and fish homozygous for the presumably null *ptch1*^{tj222} allele display elevated levels of Hh signaling activity and increased proliferation in pharyngeal chondrocytes (Koudijs et al., 2005; Hammond and Schulte-Merker, 2009). We therefore hypothesized that *ptch1* mutants might display proliferation and Op morphogenesis defects that are opposite to those observed in *ihha* mutants. In 6 dpf *ptch1* mutants, the Op appears slightly malformed with the vp edge seemingly extended relative to the other two edge lengths (Fig. 5A). As *ptch1* mutants are smaller than wild type (Koudijs et al., 2005) and Op size scales directly with standard length (Kimmel et al., 2010), we analyzed ratios of Op edge lengths to normalize for body size differences. At all time points measured, vp/jp and vp/vj edge length ratios are significantly increased in *ptch1* mutants, whereas the vj/jp edge length ratio remains unaltered (Fig. 5B). The elongation of the vp edge relative to the other edges in *ptch1* mutants is accompanied by increased cell proliferation in both *sp7:EGFP*-positive and -negative cells within two cell diameters of the vp edge (Fig. 5C,D). Together, these data indicate that active Hh signaling is sufficient to drive cell proliferation and induce growth along the vp edge.

Expression of multiple Hedgehog pathway genes is downregulated in *ihha* mutants and upregulated in *ptch1* mutants

That both *ihha* and *ptch1* mutants show localized defects in bone morphogenesis and proliferation of osteoblast precursors suggested molecular components of the Hh pathway might also be regionally restricted, so we examined this by in situ hybridization. High levels of *sp7* expression span the wild-type vp edge, matching transgenic *sp7:EGFP* expression in osteoblasts (Fig. 6A; supplementary material Fig. S2A,B). Wild-type expression of *ihha* colocalizes with *sp7* within these same cells (Fig. 6A). Lower levels of *sp7* are apparent throughout the entire Op; however, *ihha* expression appears exclusively in the more highly *sp7*-expressing osteoblasts along the vp edge (supplementary material Fig. S2C,D). Expression levels of *sp7* appear unchanged in *ihha* and *ptch1* mutants (Fig. 6B;

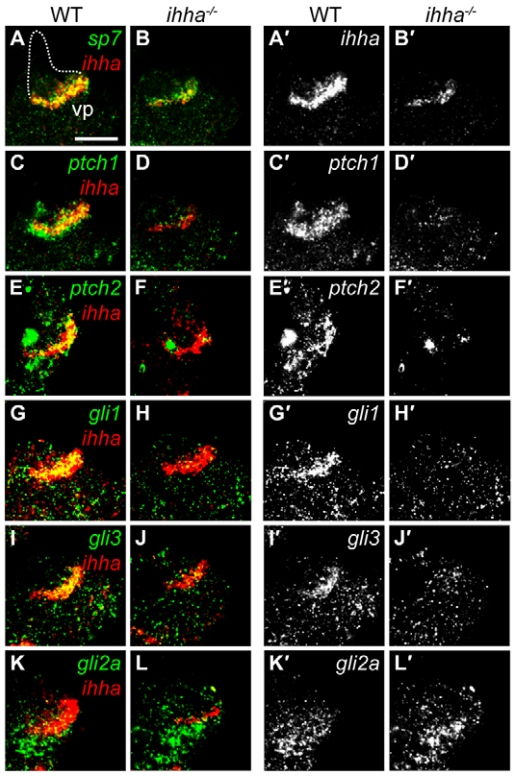

Fig. 6. Hh signaling is regionally localized. Confocal sections showing Hh pathway gene expression at 5 dpf by whole-mount in situ hybridization. Images show expression of genes relative to *ihha* (A-L) and a separated channel with individual gene expression (A′-L′) from respective images. Images are lateral views with dorsal upwards and anterior towards the left. (**A**,**A′**) *ihha* is co-expressed with *sp7* and specifically demarcates the vp edge. Other Op edges deduced by DIC are shown with a broken line. (**B**,**B′**) *sp7* expression appears similar to wild type in *ihha* mutants, although the domain may be slightly reduced, reflecting the diminished vp edge length. *ihha* expression is reduced in *ihha* mutants. (**C**,**C′**) *ptch1* is expressed ventral to vp edge osteoblasts and is also co-expressed with *ihha* along the vp edge. (**D**,**D′**) Expression of *ptch1* is lost in *ihha* mutants. (**E-F′**) *ptch2* expression resembles that of *ptch1*. (**G-J′**) *gli1* and *gli3* are co-expressed with *ihha* and their expression is decreased in *ihha* mutants. (**K-L′**) *gli2a* is expressed just ventral to the vp edge and its expression is unaltered in *ihha* mutants. Scale bar: 50 μm.

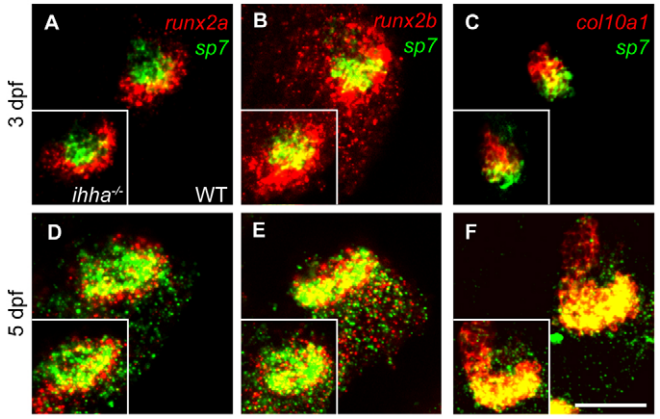

Fig. 7. Osteoblast stage markers are unaffected in *ihha* mutants. Confocal projections showing expression of osteoblast markers at 3 and 5 dpf by whole-mount fluorescent in situ hybridization. Wild-type expression is shown in the main panels and *ihha* mutant expression is shown in the insets. Images are lateral views with dorsal upwards and anterior towards the left. (**A**,**B**) At 3 dpf, *runx2a/b* expression surrounds and overlaps ventral *sp7* expression in the Op, and is unchanged in *ihha* mutants. (**C**) *col10a1* is expressed in the dorsal Op at 3 dpf and is unchanged in *ihha* mutants. (**D**,**E**) At 5 dpf, *runx2a/b* expression colocalizes with *sp7* along the vp edge and is also apparent ventral to the vp edge in non-*sp7*-expressing cells. Expression is similar in *ihha* mutants. (**F**) At 5 dpf, *col10a1* is expressed at high levels throughout the Op. The domains of these markers appear slightly reduced at 5 dpf, matching the reduction in Op size. Scale bar: 50 μm.

supplementary material Fig. S3). The *ihha* transcript in *ihha* mutants remains colocalized with *sp7* along the vp edge, albeit at seemingly decreased levels compared with wild type (Fig. 6B). We note that the *ihha*^{hu2131} allele contains a nonsense mutation; hence, the apparent decrease in *ihha* expression might be the consequence of nonsense mediated mRNA degradation (Chang et al., 2007).

To address which cells receive the Ihha signal, we investigated the expression patterns of the genes encoding the Hh signaling receptors/transcriptional targets *ptch1* and *ptch2* (Concordet et al., 1996; Lewis et al., 1999), as well as Gli genes, which are Hh signaling effectors (Ruiz i Altaba et al., 2007). At 5 dpf, wild-type expression of *ptch1* colocalizes with *ihha* in osteoblasts along the vp edge and is also apparent in cells just ventral to the *ihha*/*sp7*-expressing cells (Fig. 6C). *ptch1* expression is reduced within both of these regions in *ihha* mutants, indicating that Ihha might signal in both autocrine and paracrine manners (Fig. 6D). *ptch2* expression appears similar to *ptch1*, is reduced in *ihha* mutants and is increased in *ptch1* mutants specifically along and ventral to the vp edge (Fig. 6E,F; supplementary material Fig. S3A,B). At 5 dpf, expression of *gli1* and *gli3* in wild type colocalizes with *ihha* along the vp edge and is reduced in this region of *ihha* mutants (Fig. 6G-J). A local increase in *gli1* expression is apparent along the vp edge in *ptch1* mutants (supplementary material Fig. S3C,D). By contrast, the majority of *gli2a* expression is apparent in a broad region just ventral to the *sp7*-positive vp edge cells (Fig. 6K), and no notable changes in *gli2a* expression are visible in *ihha* or *ptch1* mutants (Fig. 6L; supplementary material Fig. S3E,F). The localized expression of *ihha* and downstream Hh signaling markers specifically in the vp edge region matches exactly where morphogenesis is altered in *ihha* and *ptch1* mutants, and supports the model that this edge of the Op is a Hh-dependent module (see Discussion).

Ordered progression through stages of osteoblast differentiation is unchanged in *ihha* mutants

Development of the bone lineage involves the sequential transition of cells through discrete stages (Bruder and Caplan, 1989; Bruder and Caplan, 1990; Li et al., 2009), and Ihh function has previously been associated with regulating osteoblast differentiation during dermal bone development (Abzhanov et al., 2007; Lenton et al., 2011). As a change to this ordered progression could result in the observed phenotypes, we looked at bone lineage markers at 3 dpf and 5 dpf. *sp7*, a marker of early osteoblasts (Li et al., 2009), is expressed at high levels in the ventral Op at 3 dpf. *runx2a* and *runx2b*, genes that encode transcription factors that directly activate

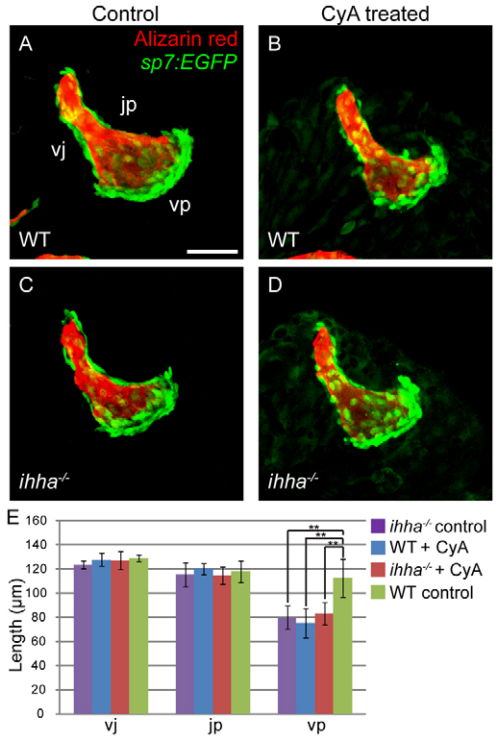

Fig. 8. Cyclopamine (CyA) induces vp edge length reduction. Confocal projections of the Op in larvae treated with CyA. Images are lateral views with dorsal upwards and anterior towards the left. (**A-C**) Wild-type larvae treated with CyA (B) display a reduction in vp edge length and phenocopy *ihha* mutants (C). (**D**) Mutants treated with CyA look similar to untreated siblings. (**E**) Measurements of vj, jp and vp edge lengths for all four treatment categories. Lengths of vj and jp are not statistically different when compared between all possible combinations of treatments. Length of the vp edge is significantly reduced in CyA-treated wild-type larvae compared with wild-type controls, but is not significantly different from *ihha* mutants treated with CyA or ethanol. Data are presented as mean±s.d., $^{**}P<0.01$ by Tukey-Kramer test, $n\geq5$ per treatment category. vp, edge connecting v and p; vj, edge connecting v and j; jp, edge connecting j and p. Scale bar: 50 μm.

and are required for *sp7* transcription (Nakashima et al., 2002; Nishio et al., 2006; Li et al., 2009), are expressed in the ventral-most *sp7*-expressing cells of the wild-type Op, as well as in pre-osteoblasts that surround the *sp7*-expressing cells (Fig. 7A,B). *col10a1*, an early osteoblast marker that persists in later-stage osteoblasts (Li et al., 2009) is co-expressed with dorsal-most *sp7* expression at 3 dpf, and also is expressed at high levels in the dorsal and presumably more mature cells of the wild-type Op (Fig. 7C). In *ihha* mutants, expression of these markers appears unchanged at 3 dpf (Fig. 7A-C, insets). The nested expression pattern of these markers at 5 dpf, when the *ihha* mutant Op phenotype is clearly apparent, is similar to the patterns observed at 3 dpf and is unchanged in *ihha* mutants (Fig. 7D-F). These data suggest that *ihha* is not required for progression through stages of osteoblast differentiation during Op morphogenesis. Notably, at both 3 and 5 dpf, the *runx2a/b* expression domain corresponds to where the Hh receptor *ptch1* is expressed and also where proliferative defects are observed in *ihha* and *ptch1* mutants, suggesting that Ihha signals to *runx2a/b*-expressing pre-osteoblasts.

Cyclopamine-treated larvae phenocopy early *ihha* mutant Op morphology

As *ihha* is expressed all along the vp edge, yet only appears to control the morphology of the most anterior region, we examined whether its co-ortholog, *ihhb*, may function redundantly with *ihha*. Expression of *ihhb* is not apparent in any bone-forming cells associated with the Op of either wild-type or *ihha* mutant larvae (supplementary material Fig. S4). However, we note that *ihhb* expression is visible in a domain just dorsal to the jp edge of the Op that corresponds to the location of muscles that elevate the Op (supplementary material Fig. S4). Thus, Ihhb could possibly signal to the posterior portion of the vp edge and compensate locally for the loss of *ihha*. Therefore, we used cyclopamine (CyA) to inhibit all Hh signaling from 4-6 dpf and test whether other Hh ligands than Ihha contribute to Op morphogenesis. We find that addition of CyA either to wild-type or *ihha* mutant larvae yields a quantitatively equivalent Op phenotype to untreated *ihha* mutants (Fig. 8). That CyA treatment matches and does not exacerbate the *ihha* mutant phenotype suggests that Ihha is the only Hh ligand required for early Op patterning and, furthermore, that the requirement for Hh signaling is during the 4-6 dpf time window, corresponding to the period of early Op morphogenesis when we first observe the *ihha* mutant phenotype.

ihha is required for proper joint formation and Op growth later in development

To assess whether morphogenetic problems persist in *ihha* mutants during later larval stages, we analyzed Op development in larvae stained vitally with Alizarin Red from 10-21 dpf. At 10 dpf, wild-type larvae display a large fanned Op that is located dorsal and lateral to the emerging subopercle (Sop) (Fig. 9A). Continual outgrowth of the vp edge causes the Op to overlap the Sop by 14 dpf (Fig. 9B). Then, the Op grows proportionally larger by 17 dpf (Fig. 9C) and eventually assumes a trapezoidal shape at 21 dpf while becoming overlapped by the interopercle (Iop) (Fig. 9D). At all of these time points, ventral, but not posterior, outgrowth of the Op is reduced in *ihha* mutants, matching our earlier observations (supplementary material Fig. S5). In addition to growth defects, *ihha* mutants display fusions between opercular dermal bones that normally form functional articulations (Hulsey et al., 2005). Approximately 64% of *ihha* mutants at 10 dpf exhibit fusions of the anterior vp edge to the adjacent dorsal edge of the Sop (Fig. 9E,I). Extension of this fusion results in nearly complete suturing of the two bones at 14 dpf (Fig. 9F). Additionally, an ectopic site of ossification of unknown origin is often apparent between the branchiostegal rays in *ihha* mutants (Fig. 9F, arrow). At 17 dpf, ~22% of *ihha* mutants have fusions between the Sop and Iop (Fig. 9G, arrow), whereas ~55% persistently exhibit Op-Sop fusions (Fig. 9I; data not shown). By this time, fusions between all three of these bones are also seen in roughly 23% of *ihha* mutants, and at 21 dpf these phenotypes continue to occur at nearly equivalent frequencies (Fig. 9H,I; data not shown).

To examine whether joint identity might be affected by the loss of *ihha* in regions of dermal bone fusions, we used a transgenic line, *trps1*^{J1271aGt} (Talbot et al., 2010) (abbreviated here to *trps1:EGFP*), which marks many skeletal joints. At 17 dpf, high *trps1:EGFP* expression is apparent ventral to the vp edge in a region that overlaps the dorsal part of the Sop (Fig. 9J, arrow). In the corresponding region of *ihha* mutants, the Op is fused to the Sop, and *trps1:EGFP* expression appears reduced (Fig. 9K). In total, these analyses demonstrate that the morphogenetic domain

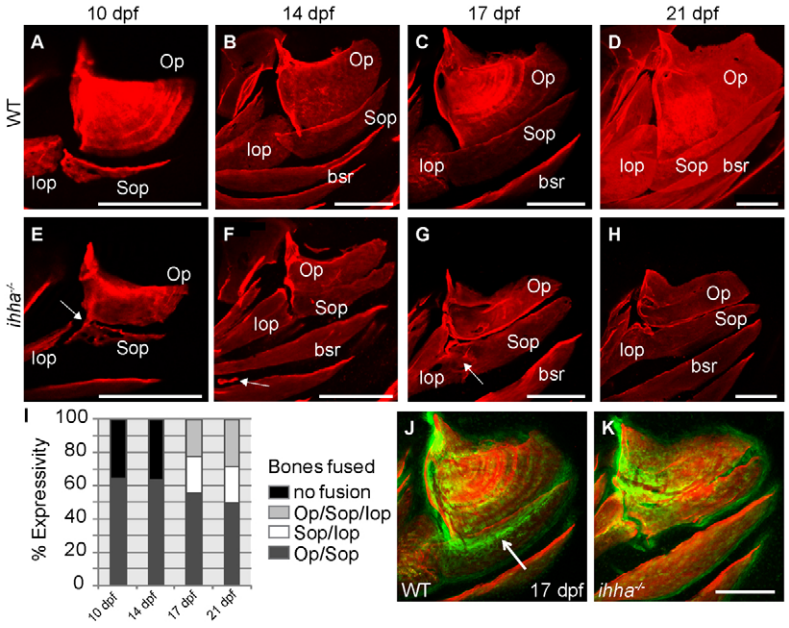

Fig. 9. *ihha* is required for proper joint formation between dermal bones. Images are lateral views with dorsal upwards and anterior towards the left. (A-H) Confocal projections of live wild-type and *ihha* mutant larvae stained with Alizarin Red. (**A-D**) Wild-type Op and adjacent bones from 10 to 21 dpf. (**E**) *ihha* mutant at 10 dpf with reduced ventral length and fusions between the ventral Op edge and dorsal Sop edge (arrow). (**F**) *ihha* mutant at 14 dpf with a nearly complete fusion of the Op and Sop, and ectopic ossification between the branchiostegal rays (arrow). (**G**) *ihha* mutant at 17 dpf with an Sop-Iop fusion (arrow), but no Op-Sop fusion. (**H**) *ihha* mutant at 21 dpf showing Iop-Sop fusion and reduced Op size. (**I**) Representation of the percentage expressivity of each fusion phenotype apparent in a single clutch of *ihha* mutants from 10 to 21 dpf. (J,K) Confocal projections of the Op stained with Alizarin Red in larvae expressing the *trps1:EGFP* transgene (green) as a joint marker. (**J**) High levels of *trps1:EGFP* expression are detectable in the dorsal Op joint and immediately ventral to the vp edge (arrow), overlapping the Sop. (**K**) *ihha* mutants with Op-Sop fusions show decreased *trps1:EGFP* expression along the presumed vp edge where the bones are now fused. bsr, branchiostegal ray; Iop, interopercle; Op, opercle; Sop, subopercle. Scale bars: 200 μm.

of *ihha* function may include the adjacent edges of dermal bones and, furthermore, suggest a function for Hh signaling in maintaining joint identity.

DISCUSSION

Hh signaling regulates cell proliferation during bone morphogenesis

Our study of opercle (Op) morphogenesis in *ihha* and *ptch1* mutant zebrafish larvae reveals that Hh signaling can regulate bone morphogenesis by control of pre-osteoblast proliferation. As determined by EdU incorporation, proliferation of cells along the ventral edge of the Op is decreased in *ihha* mutants and increased in *ptch1* mutants compared with wild-type siblings. Because we observe *runx2a/b* and *ptch1/2* expression in exactly the region of EdU incorporation, the cells receiving the Hh signal are likely to be pre-osteoblasts and incorporate EdU prior to transitioning to *sp7:EGFP*-expressing osteoblasts. This supposition is supported by our observation that early Op growth occurs largely through the recruitment, rather than division, of *sp7:EGFP*-expressing osteoblasts. Therefore, the amount of pre-osteoblast proliferation would positively correlate with Hh signaling.

Hh signaling has been linked to cell cycle control in a variety of cell types through its activation of various proto-oncogenes such as cyclins (Pasca di Magliano and Hebrok, 2003; Ehlen et al., 2006). Interaction between Ptch1 and Cyclin B1 (Barnes et al., 2001; Jenkins, 2009), as well as transcriptional regulation of various cyclin genes by Gli proteins (Kenney and Rowitch, 2000; Long et al., 2001; Yoon et al., 2002; Mill et al., 2003) are important for cell cycle progression. Because we observe the presence of Gli gene expression as well as Hh-dependent *ptch1/2* expression in cells where proliferation is altered in the *ihha* and *ptch1* mutants, it is reasonable to suppose that Ihha signaling directly stimulates pre-osteoblast proliferation through activation of cyclins. The bone fusion phenotype that we observe in later *ihha* mutant larvae might also somehow be a secondary effect of the early proliferation decrease, but this possibility requires further study.

Modular basis of Op morphogenesis

Given the localized nature of the mutant phenotypes, our study provides genetic support for the hypothesis that control of Op morphogenesis is modular (Kimmel et al., 2010). Owing to its specific dependence upon Hh signaling, vp edge morphogenesis is regulated independently from other facets of Op shaping/growth. Spatially localized control of cell proliferation by Hh signaling along the ventral Op controls two parameters of morphogenesis: vp edge length and overall ventral outgrowth. The ability of a local signal to alter specifically a local region of morphology of a given bone is consistent with the concept of dissociability, which proposes that functional or developmental units, normally integrated, might be experimentally separated from one another (Needham, 1933). Genetically based modular organization (Raff and Raff, 2000), as we observe in the Op, allows regional rates of bone growth to be individually regulated so as not to have morphogenetic consequences in other regions of the bone. Our results thus help to explain the molecular basis of allometric growth seen in many dermal bones, including the Op (Kimmel et al., 2010) (Kimmel et al., 2012). In addition, that *ihha* mutants display

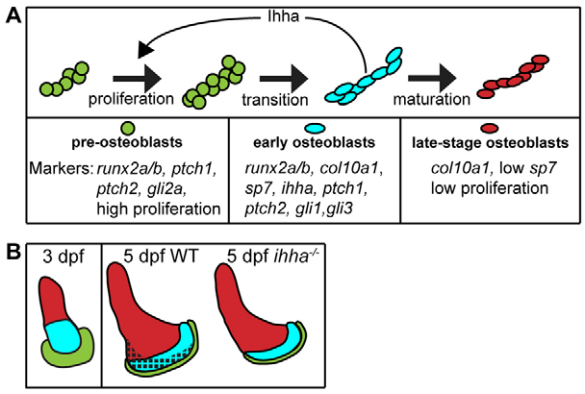

Fig. 10. Model for Hh-mediated regulation of Op morphogenesis. (**A**) Proposed model for osteoblast transition during Op development and representation of modular Op morphogenesis. A population of Hh-responsive pre-osteoblasts proliferate along the vp edge of the Op. Ihha feeds back from maturing osteoblasts to pre-osteoblasts to sustain normal rates of proliferation. Some cells within this progenitor pool subsequently are recruited to the vp edge and differentiate into *sp7/ihha*-expressing osteoblasts. These cells progressively mature, exit from the cell cycle, cease expression of *ihha*, and lessen expression of *runx2a/b* and *sp7* while maintaining *col10a1* expression. (**B**) At 3 dpf, pre-osteoblasts outline the ventral tip of the Op in both wild type and *ihha* mutants. Reduced proliferation caused by the loss of *ihha* results in a very region-specific shape change by 5 dpf, owing to a lack of pre-osteoblasts available for recruitment to the vp edge. The checkered pattern indicates the presumed Hh-dependent module of Op morphogenesis.

fusions between dermal bones that would normally articulate might mean that these adjacent regions of functionally related bones are all included in a single Hh-dependent module that extends along the lengths of the neighboring edges.

A model for how *ihha* regulates modular morphogenesis

Previous work has revealed conflicting mechanisms by which Hh signaling may regulate dermal bone development (Abzhanov et al., 2007; Lenton et al., 2011). In one study, *Ihh* gain- and loss-of-function experiments in chick and mouse suggest that Hh signaling blocks the transition of pre-osteoblasts to osteoblasts (Abzhanov et al., 2007). An opposing study reported an overall decrease in markers of osteoblast differentiation in the calvaria of *Ihh*-null mice, suggesting that Hh signaling is pro-osteogenic (Lenton et al., 2011). As we did not detect any changes in osteoblast stage markers in *ihha* mutants, our data more closely fit the pro-osteogenic model put forth by Lenton et al., as their observed reduction in osteoblast markers might reflect differences in the rate of progenitor proliferation.

In the case of the Op, we show that Ihha is secreted exclusively from *sp7*-expressing osteoblasts along the vp edge and is likely to signal to pre-osteoblasts to maintain high levels of proliferation and consequently growth along the length of the vp edge as well as ventral outgrowth (Fig. 10). Some of these proliferating pre-osteoblasts are recruited to the vp edge and subsequently transition into *sp7*-expressing osteoblasts, causing the Op to grow in a manner similar to that of other dermal bones (Wilkie, 1997; Opperman, 2000; Ramaesh and Bard, 2003). The loss of Hh signaling leads to a decrease in pre-osteoblast proliferation, which ultimately results in a reduction in vp edge length as there are fewer cells available for recruitment to the vp edge (Fig. 10). We observe the converse proliferative and morphogenetic defects in *ptch1* mutants and expect mutants for other Hh pathway repressors to exhibit similar phenotypes. Therefore, the cellular function of Hh signaling in Op morphogenesis resembles its role in cartilage morphogenesis, during which Ihh, which is secreted from pre-hypertrophic chondrocytes that have just left the proliferative pool, feeds back to maintain high levels of chondrocyte proliferation (Vortkamp et al., 1996; St-Jacques et al., 1999; Karp et al., 2000; Kronenberg, 2003). Our findings are also consistent with the pro-osteogenic role of Hh signaling in endochondral ossification (St-Jacques et al., 1999; Hammond and Schulte-Merker, 2009). Thus, Hh signaling is likely to be part of a genetic toolkit that is reused to produce similar outputs in multiple skeletogenic contexts. Importantly, our data reveal that a molecularly defined module can be restricted to a very precise region of a single bone to provide exquisite genetic control of the bone shaping process. Experimental dissociation of apparently unitary structures indicates that multiple processes must be involved in the formation of that particular structure (Raff, 1996). Accordingly, our model predicts the existence of additional modules within the Op controlled by other gene networks that regulate growth along the other edges.

Acknowledgements

We thank April DeLaurier and Mark Sasaki for dedicating their expert assistance in experimental design; Phil Ingham and Christiane Nüsslein-Volhard for providing fish strains; John Dowd and the University of Oregon fish facility for care and maintenance of animals; members of the Kimmel Lab for thoughtful conversations; Yasuko Honjo for *gli1*, *gli2a* and *gli3* probes; and Rolf O. Karlstrom for discussion of data.

Funding

This research was supported by the National Institutes of Health [R01 DE013834 and P01 HD022486 to C.B.K., F32 DE016778 to B.F.E.]. Deposited in PMC for release after 12 months.

Competing interests statement

The authors declare no competing financial interests.

Supplementary material

Supplementary material available online at
http://dev.biologists.org/lookup/suppl/doi:10.1242/dev.079806/-/DC1

References

Abzhanov, A., Rodda, S. J., McMahon, A. P. and Tabin, C. J. (2007). Regulation of skeletogenic differentiation in cranial dermal bone. *Development* **134**, 3133-3144.

Agathocleous, M., Locker, M., Harris, W. A. and Perron, M. (2007). A general role of hedgehog in the regulation of proliferation. *Cell Cycle* **6**, 156-159.

Atchley, W. R. and Hall, B. K. (1991). A model for development and evolution of complex morphological structures. *Biol. Rev. Camb. Philos. Soc.* **66**, 101-157.

Avaron, F., Hoffman, L., Guay, D. and Akimenko, M. A. (2006). Characterization of two new zebrafish members of the hedgehog family: atypical expression of a zebrafish indian hedgehog gene in skeletal elements of both endochondral and dermal origins. *Dev. Dyn.* **235**, 478-489.

Barnes, E. A., Kong, M., Ollendorff, V. and Donoghue, D. J. (2001). Patched1 interacts with cyclin B1 to regulate cell cycle progression. *EMBO J.* **20**, 2214-2223.

Bronner, F., Farach-Carson, M. C. and Roach, H. I. (2010). *Bone and Development*. London: Springer.

Bruder, S. P. and Caplan, A. I. (1989). First bone formation and the dissection of an osteogenic lineage in the embryonic chick tibia is revealed by monoclonal antibodies against osteoblasts. *Bone* **10**, 359-375.

Bruder, S. P. and Caplan, A. I. (1990). Terminal differentiation of osteogenic cells in the embryonic chick tibia is revealed by a monoclonal antibody against osteocytes. *Bone* **11**, 189-198.

Chang, Y. F., Imam, J. S. and Wilkinson, M. F. (2007). The nonsense-mediated decay RNA surveillance pathway. *Annu. Rev. Biochem.* **76**, 51-74.

Concordet, J. P., Lewis, K. E., Moore, J. W., Goodrich, L. V., Johnson, R. L., Scott, M. P. and Ingham, P. W. (1996). Spatial regulation of a zebrafish

patched homologue reflects the roles of sonic hedgehog and protein kinase A in neural tube and somite patterning. *Development* **122**, 2835-2846.
Cubbage, C. C. and Mabee, P. M. (1996). Development of the cranium and paired fins in the zebrafish *Danio rerio* (Ostrariophysi, Cyprinidae). *J. Morph.* **229**, 121-160.
Currie, P. D. and Ingham, P. W. (1996). Induction of a specific muscle cell type by a hedgehog-like protein in zebrafish. *Nature* **382**, 452-455.
DeLaurier, A., Eames, B. F., Blanco-Sanchez, B., Peng, G., He, X., Swartz, M. E., Ullmann, B., Westerfield, M. and Kimmel, C. B. (2010). Zebrafish sp7:EGFP: a transgenic for studying otic vesicle formation, skeletogenesis, and bone regeneration. *Genesis* **48**, 505-511.
Eames, B. F., de la Fuente, L. and Helms, J. A. (2003). Molecular ontogeny of the skeleton. *Birth Defects Res. C Embryo Today* **69**, 93-101.
Ehlen, H. W., Buelens, L. A. and Vortkamp, A. (2006). Hedgehog signaling in skeletal development. *Birth Defects Res. C Embryo Today* **78**, 267-279.
Flores, M. V., Tsang, V. W., Hu, W., Kalev-Zylinska, M., Postlethwait, J., Crosier, P., Crosier, K. and Fisher, S. (2004). Duplicate zebrafish runx2 orthologues are expressed in developing skeletal elements. *Gene Expr. Patterns* **4**, 573-581.
Hall, B. K. and Miyake, T. (2000). All for one and one for all: condensations and the initiation of skeletal development. *BioEssays* **22**, 138-147.
Hammond, C. L. and Schulte-Merker, S. (2009). Two populations of endochondral osteoblasts with differential sensitivity to Hedgehog signalling. *Development* **136**, 3991-4000.
Hanken, J. and Hall, B. K. (1993). *The Skull*, *Volume 1. Development*. Chicago: University of Chicago Press.
Hulsey, C. D., Fraser, G. J. and Streelman, J. T. (2005). Evolution and development of complex biomechanical systems: 300 million years of fish jaws. *Zebrafish* **2**, 243-257.
Jenkins, D. (2009). Hedgehog signalling: emerging evidence for non-canonical pathways. *Cell Signal.* **21**, 1023-1034.
Karlstrom, R. O., Talbot, W. S. and Schier, A. F. (1999). Comparative synteny cloning of zebrafish you-too: mutations in the Hedgehog target gli2 affect ventral forebrain patterning. *Genes Dev.* **13**, 388-393.
Karlstrom, R. O., Tyurina, O. V., Kawakami, A., Nishioka, N., Talbot, W. S., Sasaki, H. and Schier, A. F. (2003). Genetic analysis of zebrafish gli1 and gli2 reveals divergent requirements for gli genes in vertebrate development. *Development* **130**, 1549-1564.
Karp, S. J., Schipani, E., St-Jacques, B., Hunzelman, J., Kronenberg, H. and McMahon, A. P. (2000). Indian hedgehog coordinates endochondral bone growth and morphogenesis via parathyroid hormone related-protein-dependent and -independent pathways. *Development* **127**, 543-548.
Kenney, A. M. and Rowitch, D. H. (2000). Sonic hedgehog promotes G(1) cyclin expression and sustained cell cycle progression in mammalian neuronal precursors. *Mol. Cell. Biol.* **20**, 9055-9067.
Kimmel, C. B., Ballard, W. W., Kimmel, S. R., Ullmann, B. and Schilling, T. F. (1995). Stages of embryonic development of the zebrafish. *Dev. Dyn.* **203**, 253-310.
Kimmel, C. B., Ullmann, B., Walker, M., Miller, C. T. and Crump, J. G. (2003). Endothelin 1-mediated regulation of pharyngeal bone development in zebrafish. *Development* **130**, 1339-1351.
Kimmel, C. B., Walker, M. B. and Miller, C. T. (2007). Morphing the hyomandibular skeleton in development and evolution. *J. Exp. Zool. B Mol. Dev. Evol.* **308**, 609-624.
Kimmel, C. B., DeLaurier, A., Ullmann, B., Dowd, J. and McFadden, M. (2010). Modes of developmental outgrowth and shaping of a craniofacial bone in zebrafish. *PLoS ONE* **5**, e9475.
Kimmel, C. B, Ullmann, B., Currey, M., Hohenlohe, P. A. and Cresko, W. A. (2012). Developmental dissociation in morphological evolution of the stickleback opercle. *Evol. Dev.* (in press).
Klingenberg, C. P. (2009). Morphometric integration and modularity in configurations of landmarks: tools for evaluating a priori hypotheses. *Evol. Dev.* **11**, 405-421.
Klingenberg, C. P. (2011). MorphoJ: an integrated software package for geometric morphometrics. *Mol. Ecol. Resour.* **11**, 353-357.
Klingenberg, C. P., Mebus, K. and Auffray, J. C. (2003). Developmental integration in a complex morphological structure: how distinct are the modules in the mouse mandible? *Evol. Dev.* **5**, 522-531.
Koudijs, M. J., den Broeder, M. J., Keijser, A., Wienholds, E., Houwing, S., van Rooijen, E. M., Geisler, R. and van Eeden, F. J. (2005). The zebrafish mutants dre, uki, and lep encode negative regulators of the hedgehog signaling pathway. *PLoS Genet.* **1**, e19.
Kronenberg, H. M. (2003). Developmental regulation of the growth plate. *Nature* **423**, 332-336.
Lenton, K., James, A. W., Manu, A., Brugmann, S. A., Birker, D., Nelson, E. R., Leucht, P., Helms, J. A. and Longaker, M. T. (2011). Indian hedgehog positively regulates calvarial ossification and modulates bone morphogenetic protein signaling. *Genesis* **49**, 784-796.
Lewis, K. E., Concordet, J. P. and Ingham, P. W. (1999). Characterisation of a second patched gene in the zebrafish Danio rerio and the differential response of patched genes to Hedgehog signalling. *Dev. Biol.* **208**, 14-29.
Li, N., Felber, K., Elks, P., Croucher, P. and Roehl, H. H. (2009). Tracking gene expression during zebrafish osteoblast differentiation. *Dev. Dyn.* **238**, 459-466.
Long, F., Zhang, X. M., Karp, S., Yang, Y. and McMahon, A. P. (2001). Genetic manipulation of hedgehog signaling in the endochondral skeleton reveals a direct role in the regulation of chondrocyte proliferation. *Development* **128**, 5099-5108.
Mill, P., Mo, R., Fu, H., Grachtchouk, M., Kim, P. C., Dlugosz, A. A. and Hui, C. C. (2003). Sonic hedgehog-dependent activation of Gli2 is essential for embryonic hair follicle development. *Genes Dev.* **17**, 282-294.
Miller, C. T., Swartz, M. E., Khuu, P. A., Walker, M. B., Eberhart, J. K. and Kimmel, C. B. (2007). mef2ca is required in cranial neural crest to effect Endothelin1 signaling in zebrafish. *Dev. Biol.* **308**, 144-157.
Nakashima, K., Zhou, X., Kunkel, G., Zhang, Z., Deng, J. M., Behringer, R. R. and de Crombrugghe, B. (2002). The novel zinc finger-containing transcription factor osterix is required for osteoblast differentiation and bone formation. *Cell* **108**, 17-29.
Needham, J. (1933). On the dissociability of the fundamental process in ontogenesis. *Biol. Rev.* **8**, 180-223.
Nishio, Y., Dong, Y., Paris, M., O'Keefe, R. J., Schwarz, E. M. and Drissi, H. (2006). Runx2-mediated regulation of the zinc finger Osterix/Sp7 gene. *Gene* **372**, 62-70.
Opperman, L. A. (2000). Cranial sutures as intramembranous bone growth sites. *Dev. Dyn.* **219**, 472-485.
Parichy, D. M., Elizondo, M. R., Mills, M. G., Gordon, T. N. and Engeszer, R. E. (2009). Normal table of postembryonic zebrafish development: staging by externally visible anatomy of the living fish. *Dev. Dyn.* **238**, 2975-3015.
Parkin, C. A., Allen, C. E. and Ingham, P. W. (2009). Hedgehog signalling is required for cloacal development in the zebrafish embryo. *Int. J. Dev. Biol.* **53**, 45-57.
Pasca di Magliano, M. and Hebrok, M. (2003). Hedgehog signalling in cancer formation and maintenance. *Nat. Rev. Cancer* **3**, 903-911.
Raff, E. C. and Raff, R. A. (2000). Dissociability, modularity, evolvability. *Evol. Dev.* **2**, 235-237.
Raff, R. A. (1996). *The Shape of Life: Genes, Development, and the Evolution of Animal Form*. Chicago: University of Chicago Press.
Ramaesh, T. and Bard, J. B. (2003). The growth and morphogenesis of the early mouse mandible: a quantitative analysis. *J. Anat.* **203**, 213-222.
Ruiz i Altaba, A., Mas, C. and Stecca, B. (2007). The Gli code: an information nexus regulating cell fate, stemness and cancer. *Trends Cell Biol.* **17**, 438-447.
St-Jacques, B., Hammerschmidt, M. and McMahon, A. P. (1999). Indian hedgehog signaling regulates proliferation and differentiation of chondrocytes and is essential for bone formation. *Genes Dev.* **13**, 2072-2086.
Talbot, J. C., Johnson, S. L. and Kimmel, C. B. (2010). hand2 and Dlx genes specify dorsal, intermediate and ventral domains within zebrafish pharyngeal arches. *Development* **137**, 2507-2517.
Tyurina, O. V., Guner, B., Popova, E., Feng, J., Schier, A. F., Kohtz, J. D. and Karlstrom, R. O. (2005). Zebrafish Gli3 functions as both an activator and a repressor in Hedgehog signaling. *Dev. Biol.* **277**, 537-556.
von Dassow, G. and Munro, E. (1999). Modularity in animal development and evolution: elements of a conceptual framework for EvoDevo. *J. Exp. Zool.* **285**, 307-325.
Vortkamp, A., Lee, K., Lanske, B., Segre, G. V., Kronenberg, H. M. and Tabin, C. J. (1996). Regulation of rate of cartilage differentiation by Indian hedgehog and PTH-related protein. *Science* **273**, 613-622.
Wagner, G. P., Pavlicev, M. and Cheverud, J. M. (2007). The road to modularity. *Nat. Rev. Genet.* **8**, 921-931.
Walker, M. B., Miller, C. T., Coffin Talbot, J., Stock, D. W. and Kimmel, C. B. (2006). Zebrafish furin mutants reveal intricacies in regulating Endothelin1 signaling in craniofacial patterning. *Dev. Biol.* **295**, 194-205.
Westerfield, M. (2007). *The Zebrafish Book: a Guide for the Laboratory Use of Zebrafish (Danio rerio)*. Eugene, OR: University of Oregon Press.
Wilkie, A. O. (1997). Craniosynostosis: genes and mechanisms. *Hum. Mol. Genet.* **6**, 1647-1656.
Winata, C. L., Korzh, S., Kondrychyn, I., Zheng, W., Korzh, V. and Gong, Z. (2009). Development of zebrafish swimbladder: The requirement of Hedgehog signaling in specification and organization of the three tissue layers. *Dev. Biol.* **331**, 222-236.
Wu, S., Page, L. and Sherwood, N. M. (2006). A role for GnRH in early brain regionalization and eye development in zebrafish. *Mol. Cell. Endocrinol.* **257-258**, 47-64.
Yoon, J. W., Kita, Y., Frank, D. J., Majewski, R. R., Konicek, B. A., Nobrega, M. A., Jacob, H., Walterhouse, D. and Iannaccone, P. (2002). Gene expression profiling leads to identification of GLI1-binding elements in target genes and a role for multiple downstream pathways in GLI1-induced cell transformation. *J. Biol. Chem.* **277**, 5548-5555.
Zelzer, E. and Olsen, B. R. (2003). The genetic basis for skeletal diseases. *Nature* **423**, 343-348.